

showing that *ctl-1*, and possibly other free radical-scavenging enzymes, are required for long life-span (11). Neurons may be particularly sensitive to free radical damage during aging. In fact, overexpression of Cu/Zn SOD in only motorneurons can extend *Drosophila* life-span by 48% (3).

We propose that neuronal DAF-2 activity maintains relatively low levels of free radical-scavenging enzymes, such as SOD-3 and CTL-1, by antagonizing the DAF-16 transcription factor. Loss of DAF-2 activity from neurons, relieving the negative regulation of DAF-16, induces higher expression levels of these free radical-scavenging enzymes, thereby protecting neurons from oxidative damage. By this model, neuronal *daf-2* signaling might regulate an organism's life-span by controlling the integrity of specific neurons that secrete neuroendocrine signals, some of which may regulate the life-span of target tissues in the organism. Our results, together with those from *Drosophila*, suggest that oxidative damage to neurons may be a primary determinant of life-span.

References and Notes

1. C. E. Finch, *Longevity, Senescence, and the Genome* (Univ. of Chicago Press, Chicago, 1990).
2. K. D. Kimura, H. A. Tissenbaum, Y. Liu, G. Ruvkun, *Science* **277**, 942 (1997).
3. T. L. Parkes et al., *Nature Genet.* **19**, 171 (1998).
4. C. Kenyon, J. Chang, E. Gensch, A. Rudner, R. Tabtiang, *Nature* **366**, 461 (1993).
5. J. Z. Morris, H. A. Tissenbaum, G. Ruvkun, *Nature* **382**, 536 (1996).
6. P. S. Albert and D. L. Riddle, *Dev. Biol.* **126**, 270 (1988).
7. P. L. Larsen, P. S. Albert, D. L. Riddle, *Genetics* **139**, 1567 (1995).
8. W. A. Van Voorhies and S. Ward, *Proc. Natl. Acad. Sci. U.S.A.* **96**, 11399 (1999).
9. J. R. Vanfleteren and A. DeVreese, *FASEB J.* **9**, 1355 (1995).
10. R. S. Sohal and R. Weindruck, *Science* **273**, 59 (1996).
11. J. Taub et al., *Nature* **399**, 162 (1999).
12. S. Ogg et al., *Nature* **389**, 994 (1997).
13. S. Paradis and G. Ruvkun, *Genes Dev.* **12**, 2488 (1998).
14. S. Paradis, M. Ailion, A. Toker, J. H. Thomas, G. Ruvkun, *Genes Dev.* **13**, 1438 (1999).
15. J. Apfeld and C. Kenyon, *Cell* **95**, 199 (1998).
16. K. Ogura, M. Shirakawa, T. M. Barnes, S. Hekimi, Y. Ohshima, *Genes Dev.* **11**, 1801 (1997).
17. D. R. Hsu, P.-T. Chuang, B. J. Meyer, *Development* **121**, 3323 (1995).
18. M. Maduro and D. Pilgrim, *Genetics* **141**, 977 (1995).
19. M. Hamelin, I. M. Scott, J. C. Way, J. G. Culotti, *EMBO J.* **11**, 2885 (1992).
20. P. G. Okkema, S. W. Harrison, V. Plunger, A. Aryana, A. Fire, *Genetics* **135**, 385 (1993).
21. E. J. Aamodt, M. A. Chung, J. D. McGhee, *Science* **252**, 579 (1991).
22. Supplementary material is available at Science Online at www.sciencemag.org/feature/data/1054300.shl.
23. GFP intensity was scored in wild-type animals after 8 days of adulthood at 25.5°C. Animals with *Punc-14::GFP* or *Punc-54::GFP* showed intense GFP fluorescence that was similar to that observed at larval stages (*Punc-14::GFP*, 92% of 8-day-old adults showed high GFP intensity, *n* = 24 animals, three lines; *Punc-54::GFP*, 92% of 8-day old adults had high levels of GFP, *n* = 37 animals, one line). Animals with *Pges-1::GFP* showed a decrease in GFP intensity at adult day 8: 49% of animals showed intense/moderate GFP intensity, 27% showed low GFP intensity, and in 23% no GFP was detectable (*n* = 114 animals,

two lines). In some animals, we observed *Punc-14::GFP* expression in the pharynx and/or intestine and *Pmec-7::GFP* expression in additional neurons and one body-wall muscle.

24. Aging assays were performed at 25.5°C with agar plates containing 5-fluorodeoxyuridine (FUDR; 0.1 mg/ml) to prevent growth of progeny. Animals were grown on nematode growth medium (NGM) plates until reaching the L4 or young adult stage at 25.5°C (*age-1* strains) or at 15°C (*daf-2* strains) and then transferred to FUDR-containing plates at 25.5°C. Animals were scored every 1 to 3 days subsequently and scored as dead when they no longer responded to gentle prodding with a platinum wire. Life-span is defined as the day animals were at the L4 larval stage (time *t* = 0) until the day they were scored as dead. The results in Table 1 are the sum of at least two independent lines, except for *Pdpy-30::daf-2* and *Punc-14::daf-2*, which are from one line each.
25. Neither *Pdpy-30::age-1* or *Punc-14::age-1* can provide maternal *age-1* activity, as shown by the segregation of nontransgenic dauer-arrested animals, in contrast to the potent maternal rescue of dauer arrest in *age-1* (*m+z-*) animals. Thus, *age-1(mg44)*; *Punc-14::age-1* and *age-1(mg44)*; *Pdpy-30::age-1* animals are (*m+z+*) for *age-1* activity in the nervous system and ubiquitously, respectively. An (*m+z-*) *age-1(mg44)* animal develops into a long-lived dauer but cannot grow to reproductive adulthood, and the life-span cannot be directly compared. Thus, the rescuing activity of the strains bearing the *Punc-14::age-1* and *Pdpy-30::age-1* transgenes is underestimated by comparison with the *m+z- age-1(mg44)*, but it is the only control available.
26. L4 animals grown at 20°C were fixed in 1% parafor-

maldehyde and subjected to three freeze-thaw cycles and then incubated on ice for 10 minutes. Fixed animals were washed and dehydrated through an ethanol series before staining with Sudan Black B solution. The level of fat accumulation was scored by comparing the relative size and number and density of fat droplets in the intestine and hypodermis relative with positive [*age-1(mg44)* (*m+z-*) and *daf-2(e1370)* dauers] and negative (wild-type L4 larvae) controls.

27. Eggs were laid by gravid adults overnight at 25.5°C (*age-1* strains) or at 15°C (*daf-2* strains) and then shifted to 25.5°C. Dauer and L4 larvae or young adults were scored 3 days after egg lay. At least two independent experiments were performed for each strain, and the results from each were summed.
28. C. A. Wolkow et al., data not shown.
29. K. Kimura and G. Ruvkun, unpublished data.
30. M. W. Schwartz, S. C. Woods, D. Porte Jr., R. J. Seeley, D. G. Baskin, *Nature* **404**, 661 (2000).
31. R. N. Kulkarni et al., *Cell* **96**, 329 (1999).
32. H. Hsin and C. Kenyon, *Nature* **399**, 362 (1999).
33. Y. Honda and S. Honda, *FASEB J.* **13**, 1385 (1999).
34. We thank A. Fire, O. Hobert, J. McGhee, B. Meyer, Y. Ohshima, D. Pilgrim, and J. Sze for providing promoter plasmids; P. Delorme and Y. Liu for technical assistance; and I. Mori and members of the Ruvkun lab for helpful discussions. This work was supported in part by NIH grant AG14161. C.A.W. was supported by a postdoctoral fellowship from the Leukemia and Lymphoma Society. K.D.K. was supported by the Japanese Society for the Promotion of Science and CREST of Japan Science and Technology Corporation.

24 July 2000; accepted 18 August 2000

Structure of the Protease Domain of Memapsin 2 (β-Secretase) Complexed with Inhibitor

Lin Hong,¹ Gerald Koelsch,¹ Xinli Lin,¹ Shili Wu,¹ Simon Terzian,² Arun K. Ghosh,³ Xuenjun C. Zhang,² Jordan Tang^{1,4*}

Memapsin 2 (β-secretase) is a membrane-associated aspartic protease involved in the production of β-amyloid peptide in Alzheimer's disease and is a major target for drug design. We determined the crystal structure of the protease domain of human memapsin 2 complexed to an eight-residue inhibitor at 1.9 angstrom resolution. The active site of memapsin 2 is more open and less hydrophobic than that of other human aspartic proteases. The subsite locations from S₄ to S₂' are well defined. A kink of the inhibitor chain at P₂' and the change of chain direction of P₃' and P₄' may be mimicked to provide inhibitor selectivity.

The accumulation of the 40- to 42-residue β-amyloid peptide (Aβ) in the brain is a key event in the pathogenesis of Alzheimer's disease (AD) (1). Aβ is generated in vivo

through proteolytic cleavage of the membrane-anchored β-amyloid precursor protein (APP) by β- and γ-secretases. The γ-secretase activity, which cleaves APP within its transmembrane domain, is likely mediated by the transmembrane protein presenilin 1 (2–4). The β-secretase cleaves APP on the luminal side of the membrane and its activity is the rate-limiting step of Aβ production in vivo (5). Both proteases are potential targets for inhibitor drugs against AD. Our group (6) and others (7) recently cloned a human brain aspartic protease, memapsin 2 or BACE, and demonstrated it to be β-secretase. Memapsin

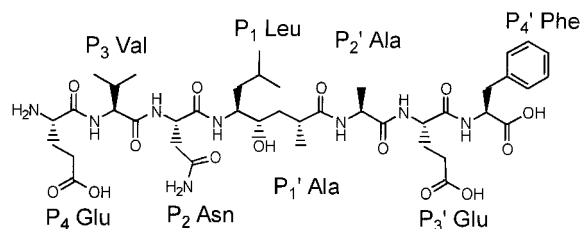
¹Protein Studies Program and ²Crystallography Program, Oklahoma Medical Research Foundation, 825 NE 13th Street, Oklahoma City, OK 73104, USA. ³Department of Chemistry, University of Illinois at Chicago, Chicago, IL 60607, USA. ⁴Department of Biochemistry and Molecular Biology, University of Oklahoma Health Sciences Center, Oklahoma City, OK 73104, USA.

*To whom correspondence should be addressed. E-mail: jordan-tang@omrf.ouhsc.edu

REPORTS

2 is a class I transmembrane protein consisting of an NH₂-terminal protease domain, a connecting strand, a transmembrane region, and a cytosolic domain (6, 7). Sequence homology with other aspartic proteases suggests that memapsin 2 has a pro sequence of about 48 residues at its NH₂-terminal region. The protease domain of pro-memapsin 2, expressed recombinantly, hydrolyzes peptides from the APP β -secretase site but has a broad specificity (6). We have used this specificity information to design potent inhibitors against this enzyme (8). OM99-2, an eight-residue transition-state inhibitor (Fig. 1) has a K_i of 1.6 nM for memapsin 2. To develop memapsin 2 inhibitors with therapeutic potential would require, besides good potency and pharmacokinetic properties, low molecular weight (<700 daltons) and high lipophilicity in order to penetrate the blood-brain barrier (9). We determined the three-dimensional structure of the memapsin 2 with an active site-bound OM99-2 at 1.9 Å resolution in order to define a template for the rational design of memapsin 2 inhibitor drugs.

Fig. 1. The chemical structure of memapsin 2 inhibitor OM99-2 with the constituent amino acids and their subsite designations. The hydroxyethylene transition-state isostere is between P₁-Leu and P₁'-Ala.



Fully active recombinant memapsin 2, which contains 21 residues of the putative pro region, residues numbers 28p–48p (10) but without the transmembrane and intracellular domains (11), was crystallized as a complex with OM99-2 (12). We report here a crystal structure of this complex at 1.9 Å resolution. The crystal structure was determined using molecular replacement methods (12) with human pepsin (22% sequence identity) as the search model. The statistical data are shown in Table 1.

The bilobal structure of memapsin 2 (Fig. 2A) has the conserved general folding of aspartic proteases (13). The inhibitor is located in the substrate binding cleft between the NH₂- and COOH-terminal lobes (10) (Fig. 2A). Active-site Asp³² and Asp²²⁸ and the surrounding hydrogen bond network are located in the center of the cleft (Fig. 2, A and B) and are conserved (14). The hairpin loop known as the “flap” (10) partially covers the cleft. The active-site carboxyls are, however, not co-planar, and the degree of deviation (50°) exceeds those observed previously. Whether this is

specific for OM99-2 binding has not been determined.

Compared to pepsin (15), the most significant structural differences are the insertions and a COOH-terminal extension in the C-lobe. Four insertions, A, C, D, and F (10) (Fig. 2, A and B), as helices and loops are located on the adjacent molecular surface near the NH₂-terminus of the inhibitor. Insertion F (10), which contains four acidic residues, forms the most negatively charged region on the molecular surface. Together, these insertions significantly enlarge the molecular boundary of memapsin 2 as compared to pepsin (Fig. 2B). These surface structural changes may function in the association of memapsin 2 with other cell-surface components. Insertions B and E are located on the molecular surface near the COOH-terminus of the inhibitor. Loop E is connected to a β -strand that is paired with part of the COOH-terminal extension. The active-site cleft of memapsin 2 is, in general, more open and accessible than that of pepsin, owing to structural differences near respective subsites P₄, P₂, and P₁' (see below) and the absence of six pepsin residues [P²⁹²TESGE²⁹⁷ (16)] at memapsin 2 residues Thr³²⁹/Gly³³⁰ on a loop opposite the flap across the active-site cleft. The 35-residue COOH-terminal extension (10) unique to memapsin 2 consists mostly of highly ordered structure (residues 359–385). Residues 369–376 form a β structure with seven hydrogen bonds to strand 293–299, whereas residues 378–383 form a helix (Fig. 2A).

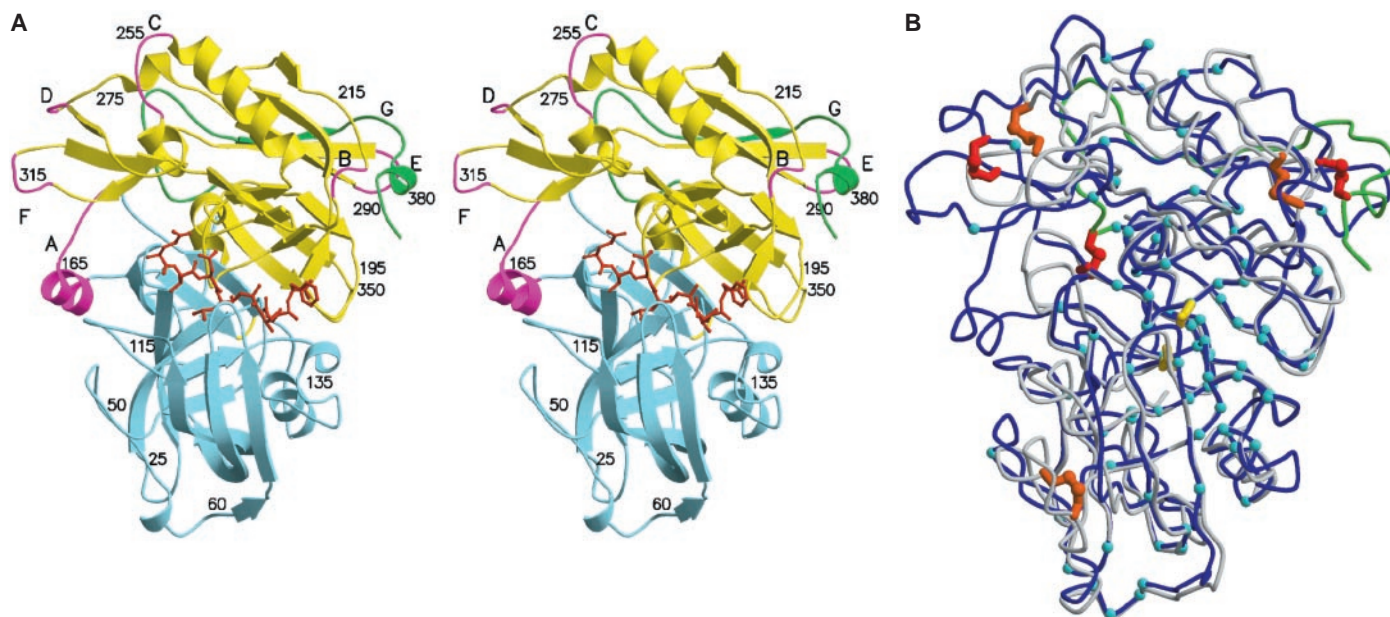


Fig. 2. The crystal structure of memapsin 2 complexed to inhibitor OM99-2. (A) Stereo view of the polypeptide backbone of memapsin 2 is shown as a ribbon diagram. The N-lobe and C-lobe are blue and yellow, respectively, except the insertion loops, designated A to G (10) in the C-lobe are magenta and the COOH-terminal extension is green. The inhibitor bound between

the lobes is shown in red. (B) The chain tracing of human memapsin 2 (dark blue) and human pepsin (gray) is compared. The light blue balls represent identical residues which are topologically equivalent. The disulfide bonds are shown in red for memapsin 2 and orange for pepsin. The COOH-terminal extension is in green. The active-site aspartic acids are shown in yellow.

REPORTS

Two of the three disulfide pairs (residues 155 and 359 and 217 and 382) unique to memapsin 2 fasten both ends of the extension region to the C-lobe. This COOH-terminal extension is longer than those observed previously for aspartic proteases and is conformationally quite different (17–20). The last eight residues (386–393) are not seen in the electron density map. Their mobility suggests the possibility of forming a short stem between the globular catalytic domain and the trans-membrane domain. Of the 21 putative pro residues present in the enzyme (10), only the last six, 43p–48p, are visible in the electron density map. The others are likely mobile, which is consistent with an unstructured pro segment

being displaced from the active-site cleft by the inhibitor (21).

The interactions of the eight-residue inhibitor OM99-2 with memapsin 2 include four hydrogen bonds between two active-site aspartates and the hydroxyl of the transition-state isostere, and ten hydrogen bonds from different parts of the binding cleft and flap to inhibitor backbone (Fig. 3). Most of these hydrogen bonds are highly conserved among eukaryotic (14, 22, 23) and HIV (24) aspartic proteases, except hydrogen bonds to Gly¹¹ and Tyr¹⁹⁸. The protease residues in contact with individual inhibitor side chains (Fig. 3) are, however, quite different compared with other aspar-

tic proteases (especially at S₃, S₁, and S₁'). Some of these differences can be traced to various insertions and deletions around the cleft. Five NH₂-terminal residues of OM99-2 are in an extended conformation and, with the exception of P₁'-Ala, all have clear contacts (within 4 Å) which define protease subsites (Fig. 3). The protease S₄ subsite is mostly hydrophilic and open to solvent. The inhibitor P₄-Glu side chain is hydrogen bonded to P₂-Asn and is also close to the Arg²³⁵ and Arg³⁰⁷ side chains (Fig. 3), which may explain why deleting this residue from OM99-2, to give the shorter inhibitor OM99-1, causes a 10-fold increase in K_i (8, 25). The protease S₂ subsite is also relatively hydrophilic and open to solvent. The hydrophilic character of the memapsin 2 S₄ and S₂ subsites is not conserved in the corresponding subsites of human aspartic proteases, such as pepsin, gastricsin, and cathepsins D and E. This difference may be utilized to design selectivity into memapsin 2 inhibitors. The relatively small S₂ residues Ser³²⁵ and Ser³²⁷ (Gln and Met, respectively, in pepsin) may accommodate an inhibitor side chain larger than P₂-Asn. The memapsin 2 S₁ and S₃ subsites, consisting mostly of hydrophobic residues, have conformations very different from pepsin due to the absence of a pepsin helix at residues 111–114 (26, 27). The

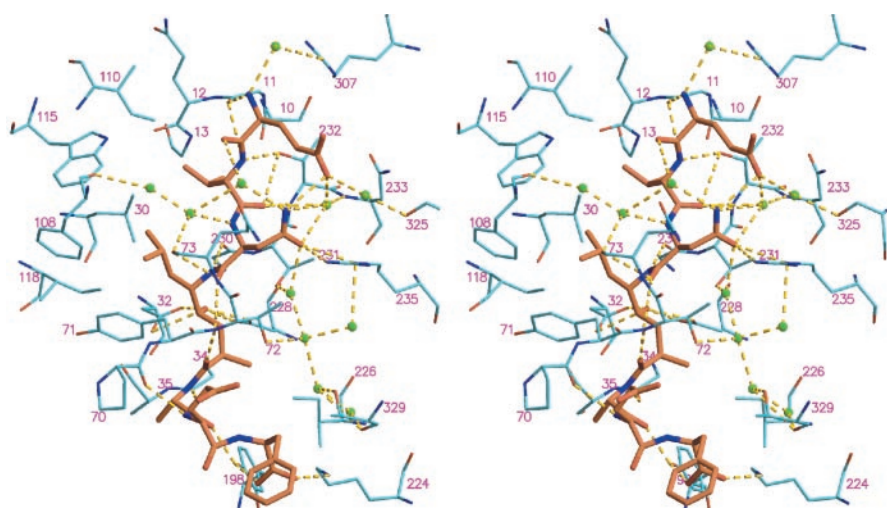


Fig. 3. Stereo presentation of interactions between inhibitor OM99-2 (orange) and memapsin 2 (light blue). Nitrogen and oxygen atoms are marked blue and red, respectively. Hydrogen bonds are indicated in yellow dotted lines. Memapsin 2 residues which comprise the binding subsites are included.

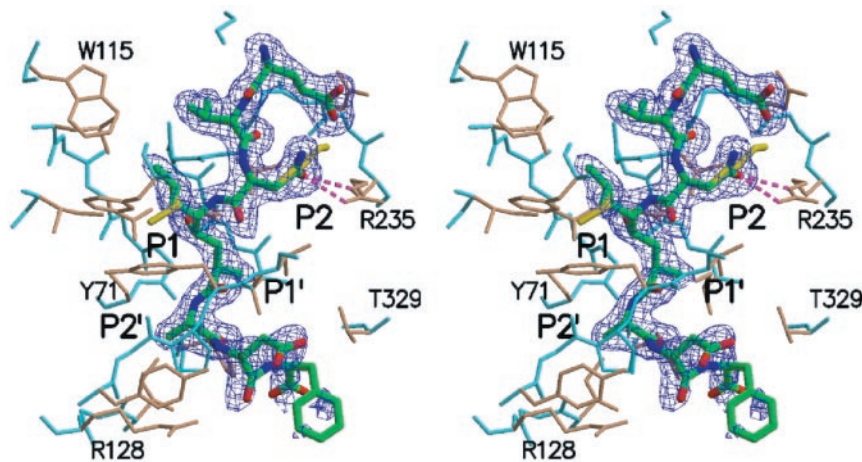


Fig. 4. Electron density of inhibitor OM99-2 and the differences in the binding of Swedish and native APP at P₁ and P₂. The omit electron density map (the $|F_o| - |F_c|$ map with the inhibitor excluded from the phase calculation), contoured at 2σ , is superimposed onto the inhibitor model with carbon atoms in green, nitrogen atoms in blue, and oxygen atoms in red. Asn and Leu side chains are those for the Swedish mutant APP at P₂ and P₁, respectively. The hydrogen bonds between inhibitor P₂ residue Asn and Arg²³⁵ are shown in magenta. The side chains of Lys and Met (in yellow) are those for the wild-type APP, and are modeled for comparison. The turn of the inhibitor backbone at P₂' is clearly visible.

Table 1. Data collection and refinement statistics.

Data statistics	
Space group	P2 ₁
Unit cell a, b, and c (Å)	53.7, 85.9, 109.2
α , β , and γ (degrees)	90.0, 101.4, 90.0
Resolution (Å)	25.0–1.9
Number of observed reflections	144,164
Number of unique reflections	69,056
R_{merge}^*	0.061 (0.25)
Data completeness (%) (25.0–1.9 Å)	90.0 (68.5)
$\langle I/\sigma(I) \rangle$	13.7 (3.0)
Refinement statistics	
$R_{\text{working}}^\dagger$	0.180
R_{free}^\ddagger	0.224
RMS deviation from ideal values	
Bond length (Å)	0.014
Bond angle (degrees)	1.8
Number of water molecules	529
Average B factor (Å ²)	
Protein	28.3
Solvent	34.0

* $R_{\text{merge}} = \sum_{\text{hkl}} \sum_i |I_{\text{hkl},i} - \langle I_{\text{hkl}} \rangle| / \sum_{\text{hkl}} \langle I_{\text{hkl}} \rangle$, where $I_{\text{hkl},i}$ is the intensity of the i th measurement and $\langle I_{\text{hkl}} \rangle$ is the weighted mean of all measurements of I_{hkl} . $^\dagger R_{\text{working}}$ (and R_{free}^\ddagger) = $\sum ||F_o| - |F_c|| / \sum |F_o|$, where F_o and F_c are the observed and calculated structure factors. Numbers in parentheses are the corresponding numbers for the highest resolution shell (2.00–1.9 Å). Reflections with $F_o/\sigma(F_o) \geq 0.0$ are included in the refinement and R factor calculation.

REPORTS

inhibitor side chains of P₃-Val and P₁-Leu are closely packed against each other and have substantial hydrophobic contacts with the enzyme (Fig. 3), especially P₁, which interacts with Tyr⁷¹ and Phe¹⁰⁸. In native APP, the P₂ and P₁ residues adjacent to the β-secretase cleavage site are Lys and Met, respectively. Swedish mutant APP has Asn and Leu in these positions, resulting in a 60-fold increase of k_{cat}/K_m over that of the native APP (6) and an early onset of AD (28). The inhibitor P₂-Asn side chain has hydrogen bonds to P₄-Glu and Arg²³⁵ (Figs. 3 and 4). Replacing P₂-Asn with Lys would result in the loss of these hydrogen bonds and the positive charge would likely interact unfavorably with the Arg²³⁵ side chain. P₁-Met would also likely have less favorable contact with the enzyme than P₁-Leu (Fig. 4). No close contact with memapsin 2 was seen for P₁'-Ala. An aspartic acid at this position, as in native APP, may be accommodated.

The direction of inhibitor chain turns at P₂' and leads P₃' and P₄' toward the protein surface (Figs. 3 and 4). As a result, the backbone of these three inhibitor residues deviates from the regular extended conformation. The side chains of P₃'-Glu and P₄'-Phe point toward the molecular surface, but have little interaction with the protease, while the terminal COOH group of P₄' has a salt bridge to Lys²²⁴ and hydrogen bonded to the hydroxyl group of Tyr¹⁹⁸. These two COOH-terminal residues have relatively high average *B* factors (56.7 Å² for P₃'-Glu and 71.9 Å² for P₄'-Phe as compared to 27.4, 22.6, 21.5, 23.7, 24.7, and 29.7 Å² for residues P₄-P₂', respectively) and poorly defined electron density, suggesting that they are relatively mobile. In contrast, the S₃' and S₄' subsites in renin-inhibitor (CH-66) complex (23) have a defined structure. The topologically equivalent region of these renin subsites (residues 293–298 in pepsin numbering) is absent in memapsin 2. The conformation of P₂' to P₄', including a kink at P₂' and the change of backbone direction at P₃' and P₄', is rare in aspartic protease inhibitors. The backbone turn at P₂' is likely caused by a hydrogen bond between P₂' carbonyl and hydroxyl of Tyr¹⁹⁸, not seen in the inhibitor complexes of renin (23) and endothiapepsin (22). A similar hydrogen bond is present in pepsin and a similar P₂' kink has been observed for one of its inhibitors (27). The conformation of the three COOH-terminal residues of OM99-2, including the kink at the P₂' backbone, may be a way to direct a long protein substrate out of the active-site cleft.

The well-defined subsite structures spanning P₄ to P₂' provide a template for rational design of drugs against memapsin 2. The unusual conformation of subsites

P₂', P₃', and P₄' may facilitate the design of inhibitors selective for memapsin 2.

References and Notes

1. D. J. Selkoe, *Nature* **399A**, 23 (1999).
2. M. S. Wolfe *et al.*, *Nature* **398**, 513 (1999).
3. Y.M. Li *et al.*, *Nature* **405**, 689 (2000).
4. W. P. Esler *et al.*, *Nature Cell Biol.* **2**, 428 (2000).
5. S. Sinha and I. Lieberburg, *Proc. Natl. Acad. Sci. U.S.A.* **96**, 11049 (1999).
6. X. Lin *et al.*, *Proc. Natl. Acad. Sci. U.S.A.* **97**, 1456 (2000).
7. β-Secretase was reported as, besides memapsin 2 (6), also (i) BACE [R. Vassar *et al.*, *Science* **286**, 735 (1999)], (ii) Asp 2 [R. Yan *et al.*, *Nature* **402**, 533 (1999)], (iii) membrane-bound aspartic proteinase [S. Sinha *et al.*, *Nature* **402**, 537 (1999)], and (iv) Asp 2 [I. Hussain *et al.*, *Mol. Cell. Neurosci.* **14**, 419 (1999)].
8. OM99-2 is based on an octapeptide sequence of Glu-Val-Asn-Leu-Ala-Ala-Glu-Phe in which the Leu-Ala bond is substituted by a hydroxyethylene transition-state isostere (25). The *K_i* value reported for recombinant pro-memapsin 2 (6) was 9.8 nM (25). The *K_i* value for recombinant memapsin 2 used in this structural study has been determined to be 1.6 nM (27).
9. B. P. Kearney and F. T. Aweeka, *Neurol. Clin.* **17**, 883 (1999).
10. The putative pro residues 28p–48p present in memapsin 2 used for structural determination are LRL-PRETDEEPEEPGRRSFV. The alignment of amino acid sequences and secondary structures of memapsin 2 and human pepsin is shown in an additional Web figure (29). The numbering of residues in memapsin 2 used in this paper starts at Glu¹ in the sequence of EMVDN- and continues based on the published memapsin 2 sequence (6). The positions and marker sequences of the regions discussed in the text (insertions A through G) are: NH₂-terminal lobe, residues 1–180, starting at Glu¹ to the end of sequence IGGID¹⁸⁰; COOH-terminal lobe, residues 181–385, starting at His¹⁸¹ in the sequence of HSLYT to the end of COOH-terminal extension G (see below); flap residues, VPYTQGK (residues 69–75); insertion A, GFPLNQSEVL (residues 158–167); insertion B, KEYN (residues 218–221); insertion C, ASSTEKFP (residues 251–258); insertion D, WQAG (residues 270–273); insertion E, EVTNQS (residues 290–295); insertion F, DVATSQD (residues 311–317); and COOH-terminal extension G, CHVHDEFRTAAVEGPFVTLDMEDCGYNI-PQTDEST (residues 359–393).
11. Residues 1p to 393 of human pro-memapsin 2 [residues 28p to 393 are shown in additional Web figure (29)]; the complete pro sequence is described in (6)] was expressed from vector pET11a using an *Escherichia coli* host BL21(DE3) as previously described (6). The inclusion bodies were harvested, washed, and dissolved in 0.1 M Tris, 1 mM EDTA, 1 mM glycine, 8 M urea, and 0.1 M β-mercaptoethanol (pH 10), and then refolded by rapid dilution as previously described (30). The recombinant pro-memapsin 2 was purified by gel filtration on Sepharose S-300 and FPLC on Resource-Q (Pharmacia) column (30). The NH₂-terminal sequence of purified memapsin 2 established that it started at Leu^{28p} with a minor component starting at Leu^{30p}. Since the expressed pro-memapsin 2 had been determined to contain 48 putative pro residues [starting at the sequence of Ala-Gly-Val-Leu- (6)], activation with the removal of part of the pro peptide (residues 1p to 28p or 30p) had taken place during the preparation procedure. This purified enzyme form has the highest specific activity [using the assay described in (25); see also (6)] among all the activated memapsin 2 (21).
12. Purified recombinant memapsin 2 in the presence of fivefold molar excess of OM99-2 was crystallized in 0.2 M ammonium sulfate and 22.5% PEG 8000 buffered with 0.1 M Na-cacodylate (pH 7.4) at 20°C, using the hanging drop vapor diffusion method. The typical crystal size was about 0.4 mm by 0.4 mm by 0.2 mm. Diffraction data were collected at 95 K with an Raxis-IV image plate, integrated and reduced with the HKL program package [Z. Otwinowski and W. Minor, *Methods Enzymol.* **276**, 307 (1997)]. The crystals belong to the space group P2₁ with two memapsin 2/OM99-2 complexes per crystallographic asymmetric unit and 56% solvent content. The molecular replacement calculations were performed using pepsin (Protein Data Bank accession number 1psn) as the search model with the program AMoRe [J. Navaza, *Acta Crystallogr. A* **50**, 157 (1994)]. The refinement was carried out using the program CNS (31)]. The molecular graphic program O [T. A. Jones, J. Y. Zou, S. W. Cowan, M. Kjeldgaard, *Acta Crystallogr. A* **47**, 110 (1991)] was used for interactive map fitting. The initial solution had a correlation coefficient of 22% and an *R* factor of 0.51 for data in the range of 15 to 3.5 Å. The $|F_o| - |F_c|$ omit map from early stages of refinement revealed surplus electron density within the active-site cleft, which was fitted with the inhibitor structure. After multiple cycles of refinement and model building, the *R_{working}* and *R_{free}* values of the final structure were 18.0 and 22.4%, respectively. Crystallographic refinement used molecular dynamics and energy minimization functions of CNS (31). No solvent molecules were added to the model until the *R* factor was reduced below 0.25. Solvent molecules, 529, were then added as identified in the $|F_o| - |F_c|$ map contoured at the 3 σ level. Noncrystallographic symmetry restriction and averaging were used in early stages of refinement and model building. Bulk solvent and anisotropic overall *B* factor corrections were applied through the refinement. In the final model, no backbone φ, ψ torsion angles were located in the disallowed region of the Ramachandran plot whereas 90% of the residues were located in the most favored regions, as defined by the program PROCHECK [R. A. Laskowski, M. W. MacArthur, D. S. Moss, J. M. Thornton, *J. Appl. Crystallogr.* **26**, 283 (1993)]. The two memapsin 2/OM99-2 complexes in the crystallographic asymmetric unit are essentially identical.
13. J. Tang, M. N. James, I. N. Hsu, J. A. Jenkins, T. L. Blundell, *Nature* **271**, 618 (1978).
14. D. R. Davies, *Annu. Rev. Biophys. Biophys. Chem.* **19**, 189 (1990).
15. A. R. Seileki, A. A. Fedorov, A. Boodhoo, N. S. Andreeva, M. N. James, *J. Mol. Biol.* **214**, 143 (1990).
16. Single-letter abbreviations for the amino acid residues are as follows: A, Ala; C, Cys; D, Asp; E, Glu; F, Phe; G, Gly; H, His; I, Ile; K, Lys; L, Leu; M, Met; N, Asn; P, Pro; Q, Gln; R, Arg; S, Ser; T, Thr; V, Val; W, Trp; and Y, Tyr.
17. S. M. Cutfield *et al.*, *Structure* **3**, 1261 (1995).
18. C. Abad-Zapatero *et al.*, *Protein Sci.* **5**, 640 (1996).
19. J. Symersky, M. Monod, S. I. Foundling, *Biochemistry* **36**, 12700 (1997).
20. J. Yang and J. W. Quail, *Acta Crystallogr. D* **55**, 625 (1999).
21. J. Ermolieff, J. A. Loy, G. Koelsch, J. Tang, *Biochemistry*, in press.
22. D. Bailey and J. B. Cooper, *Protein Sci.* **3**, 3129 (1994).
23. C. G. Dealwis *et al.*, *J. Mol. Biol.* **236**, 342 (1994).
24. A. Wlodawer and J. W. Erickson, *Annu. Rev. Biochem.* **62**, 343 (1993).
25. A. Ghosh *et al.*, *J. Am. Chem. Soc.* **122**, 3522 (2000).
26. M. Fujinaga, M. M. Chernaia, N. I. Tarasova, S. C. Mosimann, M. N. James, *Protein Sci.* **4**, 960 (1995).
27. M. Fujinaga *et al.*, *Acta Crystallogr. D* **56**, 272 (2000).
28. M. Mullan *et al.*, *Nature Genet.* **2**, 340 (1992).
29. Supplementary Web figure is available at www.sciencemag.org/feature/data/1052536.shl.
30. X. Lin, Y. Lin, J. Tang, *Methods Enzymol.* **241**, 195 (1994).
31. A. T. Brünger *et al.*, *Acta Crystallogr. D* **54**, 905 (1998).
32. We thank D. R. Davies, A. Wlodawer, and J. D. Capra for critical reading of this manuscript, and D. Downs and A. Irwin for assisting in enzyme preparation. Coordinates have been deposited in the Protein Data Bank (accession number 1FKN). J.T. is holder of the J. G. Puterbaugh Chair in Biomedical Research at the Oklahoma Medical Research Foundation. G.K. is a Scientist Development Awardee of the American Heart Association.

24 May 2000; accepted 17 August 2000